Available online at www.sciencedirect.com
ScienceDirect
Journal of Power Sources 176 (2008) 444–451
JOURNAL OF POWER SOURCES
www.elsevier.com/locate/jpowsour

Carbon support oxidation in PEM fuel cell cathodes

S. Maass [a], F. Finsterwalder [a,*], G. Frank [a], R. Hartmann [a], C. Merten [b]

[a] *Department of MEA and Stack Technology, DaimlerChrysler AG, Wilhelm-Runge-Str. 11, 89081 Ulm, Germany*
[b] *Institute for Chemical Engineering (ICVT), University of Stuttgart, Boeblinger Str. 72, 70199 Stuttgart, Germany*

Available online 25 August 2007

Abstract

Oxidation of the cathode carbon catalyst support in polymer electrolyte fuel cells (PEMFC) has been examined. For this purpose platinum supported electrodes and pure carbon electrodes were fabricated and tested in membrane-electrode-assemblies (MEAs) in air and nitrogen atmosphere. The in situ experiments account for the fuel cell environment characterized by the presence of a solid electrolyte and water in the gas and liquid phases. Cell potential transients occurring during automotive fuel cell operation were simulated by dynamic measurements. Corrosion rates were calculated from CO_2 and CO concentrations in the cathode exhaust measured by non-dispersive infrared spectroscopy (NDIR). Results from these potentiodynamic measurements indicate that different potential regimes relevant for carbon oxidation can be distinguished. Carbon corrosion rates were found to be higher under dynamic operation and to strongly depend on electrode history. These characteristics make it difficult to predict corrosion rates accurately in an automotive drive cycle.

Keywords: Polymer electrolyte membrane fuel cell; Carbon corrosion; Catalyst support degradation

1. Introduction

PEM fuel cell systems running on hydrogen are seen as a future alternative to conventional combustion engines for automotive application. While first fuel cell products for off-grid power supply are already commercially available, market launch of transportation applications is delayed due to tough requirements regarding costs, power density, robustness and long-term stability.

Platinum is still the only known catalyst material providing sufficiently high activity for the oxygen reduction reaction. To reduce the amount of precious metal used, platinum is usually supported on carbon in the form of nano-dispersed particles. This dispersement allows for high-catalyst surface areas at low-catalyst loadings. Carbon supported catalysts are, however, susceptible to catalyst particle agglomeration. Another major drawback of high-performance, low-loaded electrodes resides in the thermodynamic instability of carbon under PEMFC cathode conditions [1]. Above 0.207 V versus NHE carbon can be oxidized to carbon dioxide following reaction (1). Oxidation to carbon monoxide (2) is thermodynamically not favoured according to reaction (3):

$$C + 2H_2O \rightarrow CO_2 + 4H^+ + 4e^-, \quad \varphi_{00} = 0.207\,V \tag{1}$$

$$C + H_2O \rightarrow CO + 2H^+ + 2e^-, \quad \varphi_{00} = 0.518\,V \tag{2}$$

$$CO + H_2O \rightarrow CO_2 + 2H^+ + 2e^-, \quad \varphi_{00} = -0.103\,V \tag{3}$$

Oxidation of carbon support – generally referred to as carbon corrosion – can lead to performance decrease due to accelerated loss of active surface area [2] and alteration of pore morphology and pore surface characteristics [3]. Support degradation can be initiated under conditions where the electrode is exposed to high-electrochemical potentials, as is the cathode at high-cell potentials. In automotive applications this generally corresponds to low-electric power demand, which makes up a significant portion of the fuel cells total operational time. Two distinct states of operation have to be considered separately, resulting in extremely strong performance decay due to corrosion incidents. The first state is characterized by complete fuel starvation of one or more cells in a working stack. The starved cells are driven into reversed operation with the anode potential being higher than the cathode potential. This state entails water electrolysis and carbon oxidation on the fuel cell anode in order to provide the required protons and electrons for the reduction of oxygen on the cathode. Sustaining the stack current results in massive oxidation of the anode catalyst support. Cell reversal manifests

* Corresponding author. Tel.: +49 731 505 2995; fax: +49 711 3052 137725.
E-mail address: florian.finsterwalder@daimlerchrysler.com
(F. Finsterwalder).

0378-7753/$ – see front matter © 2007 Elsevier B.V. All rights reserved.
doi:10.1016/j.jpowsour.2007.08.053

itself in negative cell voltage which can drop as low as −2.0 V [4]. The second state of irregular high-electrode potentials is characterized by partial fuel starvation of the active anode area of an individual cell in the stack. This condition may be caused either by local undersupply of hydrogen [5,6] or a hydrogen-air front passing over the active area during start up and shut down of the fuel cell [6,7]. Because oxygen-permeation from the cathode over the membrane into the anode compartment cannot be prevented, oxygen is present in the hydrogen deficient areas on the anode. As a consequence, potential shifts can occur caused by a drop of the in-plane membrane potential. This mechanism was already described for phosphoric acid fuel cells (PAFC) [8] and has recently been verified and simulated for PEM fuel cells [6,9]. Complete cell reversal and local fuel starvation both result in significant performance losses within a couple of minutes and must be continuously ruled out, e.g. by an appropriate operating strategy and by choice of adequate electrode materials [9–11].

Potentiostatic electrooxidation of carbon supports under PAFC conditions has been intensely studied in the literature [12–16]. Gas diffusion electrodes immersed in liquid electrolyte have been used to simulate PEM fuel cell conditions [3]. Gas phase oxidation has been regarded as an accelerated test to evaluate carbon materials for use as catalyst support in low-temperature fuel cells [17]. Few literature is, however, available on carbon corrosion in real PEM fuel cell environment under potentiodynamic operating conditions. Willsau and Heitbaum made a very thorough analysis of carbon oxidation in gas diffusion electrodes in liquid electrolyte under potential sweep operation [18]. They measured an accelerating effect of platinum on corrosion rates and were able to identify several oxidation peaks by differential electrochemical mass spectroscopy (DEMS). Roen et al. got similar results with PEMFC electrodes in helium atmosphere but did not offer an explanation for all observed phenomena [19].

The scope of this paper is to evaluate carbon support oxidation under potential transients in realistic PEM fuel cell environment, i.e. in the presence of a solid ionomer electrolyte and water in both the gas and liquid phases. All experiments were therefore conducted in situ using membrane-electrode-assemblies. Carbon corrosion was measured by monitoring the evolution of carbon dioxide and carbon monoxide at the cell outlet.

2. Experimental

In-house fabricated membrane-electrode-assemblies were employed for all measurements. Catalyst and support materials to be evaluated were incorporated in the cathode catalyst layer. The results presented in this paper are based on pure Ketjenblack EC300J®-electrodes (Akzo Nobel, 736 $m^2\,g^{-1}$ BET surface area measured, literature value 930 $m^2\,g^{-1}$ [20]) and Ketjenblack-supported platinum-electrodes (50% Pt/C, Tanaka). Both materials were purchased in powder form and catalyst inks were prepared with 20 wt% Nafion® solution (EW1100, DuPont) and additional organic solvents. Catalyst layers were directly coated on 25 μm Nafion® membranes. Hot pressing of the catalyst-coated-membranes (CCMs) with in-house fabricated gas diffusion layers (GDLs) based on Toray TGP-H60 gave the five layer-MEAs used in this work. In all cases the anode was based on a Pt/C-catalyst at high loading (1.0 mg cm^{-2}) serving both as a counter and reference electrode. The excessive catalyst loading in combination with the reversibility of hydrogen oxidation keep the anode overpotential close to the reversible hydrogen potential. All potentials given in this paper refer to the anode potential.

Fuel cell experiments were conducted in lab-scale cells of 45 cm^2 active area on standard test benches with digital control of mass flows, humidification and temperature. Pt/C-MEAs were conditioned at 80 °C cell temperature and 40% relative humidity over night until stable cell voltage was observed. MEAs with pure carbon cathodes were held potentiostatically at similar potentials observed with Pt-activated electrodes and conditioned with higher humidity to account for the lack of product water. An IM6 Electrochemical Workstation (Zahner elektrik) was used to control cell potentials. Potentiodynamic measurements were conducted with a slew rate of 2 mV s^{-1} for six repeating cycles to ensure steady-state conditions. The supplied gases were research grade hydrogen on the anode and nitrogen or synthetic air (20% oxygen in nitrogen) on the cathode. Cell temperature was 85 °C and gases were fully humidified if not mentioned otherwise.

Corrosion rates were calculated from the evolution of carbon mono- and di-oxide and converted into a mass flux of carbon in $\mu g_C\,h^{-1}\,cm^{-2}$. CO_x-concentrations were monitored at the cathode cell outlet by means of a NGA2000 non-dispersive infrared spectrometer (Emerson Process). IR spectroscopy allows to measure concentrations of CO_2 and CO in the range of ppm even in nitrogen and oxygen atmosphere, i.e. during fuel cell operation.

Retention time and peak height correction factors were determined by CO-stripping experiments with platinum black electrodes. Reference tests on MEAs without cathode catalyst layer (but with cathode GDL including micro-diffusion layer) were conducted to identify background noise from gases, test equipment or other MEA components besides the catalyst layers. Only concentrations of about one thousandth of typical corrosion signals could be detected and background noise thus was regarded as negligible. The low-oxidation rates of the carbonaceous GDL-backing and the micro-diffusion layer can be explained by the lack of ionic contact which is required for the electrochemical oxidation of carbon.

3. Theory

As already stated in Section 1, carbon is used as support for the active fuel cell catalyst component, usually platinum or platinum alloys. The surface area per unit weight of noble metal is increased by keeping it in a dispersed condition. Sp^2-hybridized carbon is the most commonly used support material because of its high-electrical conductivity, its good processability and its availability in a wide variety of particle morphologies [21]. Furthermore carbon shows relatively high chemical and thermal stability compared to other support materials used in heterogeneous catalysis, like alumina and silica for example [22]. Common supports are carbon blacks like Vulcan XC-72® (Cabot Corp.) or Ketjenblack EC300J®.

Carbon blacks are manufactured by pyrolysis of liquid or gaseous hydrocarbons. They exhibit a three-dimensional structure of microcrystalline primary particles (20–50 nm in diameter) aggregated to amorphous clusters. Because of their heterogeneous structure the primary particles exhibit a high density of surface defects. These defects represent crystallographic sites of different activity for the adsorption of surface species, mainly hydrogen and oxygen functional groups. In the literature phenol, carboxyl, carbonyl, quinone and lactone groups were identified [23]. Carbon oxidation also starts at edges and corners of basal planes since these exhibit unsaturated valences and free σ-electrons [24]. Surface oxides are regarded as reaction intermediates of the corrosion mechanism that can simplified be written as the formation of surface functional groups above 0.207 V versus NHE (4), followed by subsequent oxidation to carbon dioxide [12]:

$$C + H_2O \rightarrow C\text{–}O_{ad} + 2H^+ + 2e^-, \quad \varphi_{00} = 0.207\,V \qquad (4)$$

$$C\text{–}O_{ad} + H_2O \rightarrow CO_2 + 2H^+ + 2e^- \qquad (5)$$

The detailed mechanism is not yet fully understood but is presumed to include parallel formation of surface and gaseous carbon oxides by disproportion of oxygen functional groups [25].

4. Results and discussion

Dynamic measurements and measurements at constant potential were conducted at varied temperature and humidity and in different potential windows. Carbon dioxide evolution could be detected on Pt/C- as well as on pure C-electrodes. In contrast to that, carbon monoxide was only formed on pure carbon electrodes and only in concentrations of one tenth of carbon dioxide (see, e.g. Fig. 3). In presence of platinum carbon monoxide could not be detected because it is adsorbed on the metal surface at potentials below 0.55 V. At higher potentials CO is oxidized to CO_2 according to reaction (6), i.e. platinum accelerates the adjustment of the thermodynamic equilibrium.

$$Pt\text{–}CO_{ad} + Pt\text{–}OH_{ad} \rightarrow Pt_2 + CO_2 + H^+ + e^- \qquad (6)$$

4.1. Identification of corrosion processes

In Figs. 1 and 2 measurements on pure carbon and on platinum-activated carbon electrodes are compared in air and nitrogen, respectively. The upper half of the diagrams shows corrosion rates that were calculated from measured CO_x concentrations. Lower parts show the current response of the electrodes. In case of measurements in nitrogen atmosphere the curves represent cyclic voltammograms governed by double layer charging currents and by formation and oxidation/reduction of hydrogen and oxygen surface layers. In case of measurements in air the current is dominated by Faradayic oxygen reduction currents that approach a limiting current since flow rates were held constant. Faradayic carbon oxidation currents themselves cannot be resolved because they are only in the order of $\mu A\,cm^{-2}$ and thus

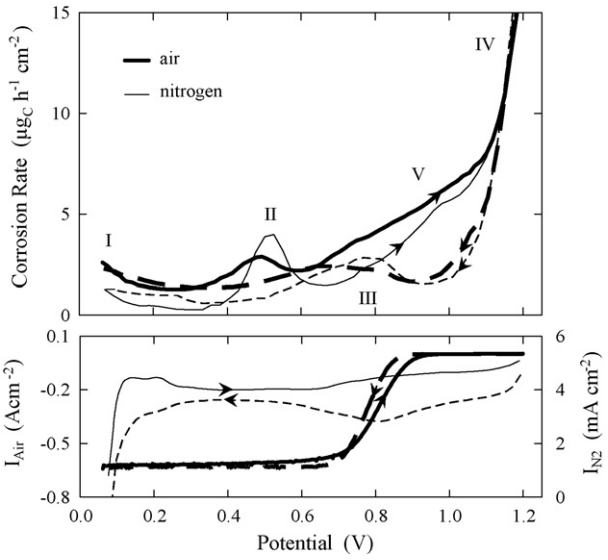

Fig. 1. Potentiodynamic corrosion measurements on Pt/C-electrodes in air (thick lines) and nitrogen (thin lines). The upper half of the diagram shows CO_2 evolution (CO was not measured on Pt/C-electrodes), the lower half shows current response, i.e. cyclic voltammograms in case of measurements in nitrogen and polarization curves in case of air measurements. Solid lines show respective anodic sweeps, dashed lines show cathodic sweeps.

at least three orders of magnitude lower than currents resulting from the other surface processes.

Corrosion rates in air and nitrogen show same trends though they are somewhat higher in air. Considering the dependence of carbon corrosion on humidity (as shown later), this is mainly due to product water formation during air-operation. From Pt/C-electrodes five distinct maxima of CO_2 evolution can be detected (Fig. 1) while pure C-electrodes only exhibit two maxima (Fig. 2). These maxima are numbered as shown in the figures,

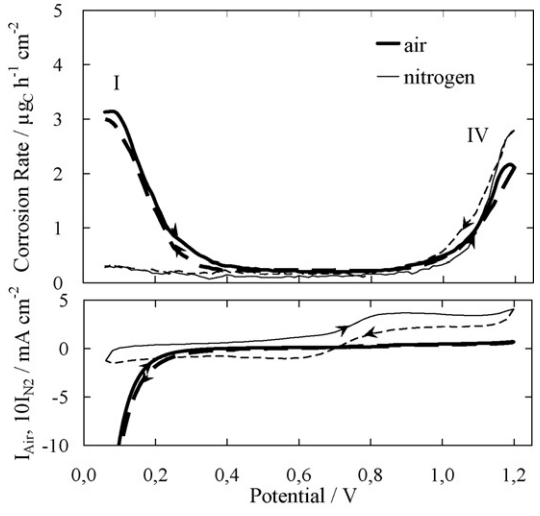

Fig. 2. Potentiodynamic corrosion measurements on carbon electrodes in air (thick lines) and nitrogen (thin lines). The upper half of the diagram shows total carbon corrosion rate as sum of CO_2 and CO evolution, the lower half shows corresponding currents, i.e. cyclic voltammograms in case of measurements in nitrogen and polarization curves in case of air measurements. Solid lines show respective anodic sweeps, dashed lines show cathodic sweeps.

with peaks I and IV being the cathodic and anodic maxima, respectively. Peak II is located at 0.55 V in the anodic cycle, Peak III at 0.75 V in the cathodic cycle of Pt/C-measurements. These peaks cannot be detected from pure carbon electrodes. With new electrodes feature V appears only as a shoulder, broadening the anodic branch of peak IV. In the following the different distinct maxima and their underlying processes are analysed.

Peak IV is characterized as an exponential increase of the corrosion rate at the anodic potential limit. For pure carbon electrodes this peak develops above 0.9 V and can be attributed to electrochemical carbon oxidation according reaction (1) and (2). Though oxygen functional groups are formed on carbon at potentials as low as 0.207 V (4), oxidation of these intermediates is highly irreversible on pure carbon and therefore reaction (5) requires a high overvoltage [25]. For Pt/C-electrodes peak IV seems to enhance background corrosion from about 0.3 V on, i.e. the onset of reaction (5) is shifted from 0.9 V at pure carbon electrodes to that decidedly lower potential. Platinum catalyses the carbon oxidation reaction as reported in the literature [18] and significantly reduces overvoltage for reaction (5). This leads to an increase in corrosion rates compared to that of pure carbon electrodes (Fig. 2). The catalytic effect might be due to participation of platinum oxide groups which reduce overvoltage by enabling a reaction similar to (7).

$$C\text{–}O_{ad} + Pt\text{–}OH_{ad} \rightarrow \ Pt \ + \ CO_2 + H^+ + e^- \qquad (7)$$

Peak III is detected in the down-going potential sweep from the anodic limit of Pt/C-electrodes. Since it cannot be detected on pure C-electrodes, platinum must play a role in the underlying process. Comparison with the cyclic voltammogram shows that peak III coincides with the reduction of oxygen-containing surface groups on platinum. Obviously hydroxyl surface groups on platinum, which are destabilized at lower electrode potentials [26], do not only react with protons to water but also combine with carbon surface groups to carbon dioxide. Peak III will be further discussed in Section 4.2 by examining the influence of the upper potential limit.

Peak I at the cathodic potential limit was found from Pt/C-electrodes in air as well as in nitrogen and also from C-electrodes in air. On pure carbon electrodes in nitrogen atmosphere no increase in CO_x-evolution was seen in this potential range. Corrosion rates were highest from C-electrodes in air, followed by CO_2-evolution from Pt/C in air and then Pt/C in nitrogen. Since the potential range of peak I lies below the reversible potential of electrochemical carbon oxidation, another process ought to be responsible for the corrosion monitored. It is conjectured that chemical oxidation of carbon by hydrogen peroxide is the underlying process of peak I. Hydrogen peroxide can be formed on both types of electrodes in the potential region of peak I. Though platinum mainly promotes direct oxygen reduction to water, it is known from RRDE experiments that peroxide species are produced during oxygen reduction on supported as well as on unsupported platinum in the potential region of hydrogen adsorption [27–29]. Zinola et al. have measured very low H_2O_2 production in nitrogen atmosphere [30]. In contrast to the reaction on platinum, oxygen reduction on carbon mainly proceeds through the $2\,e^-$-pathway which leads to formation of hydrogen peroxide [31].

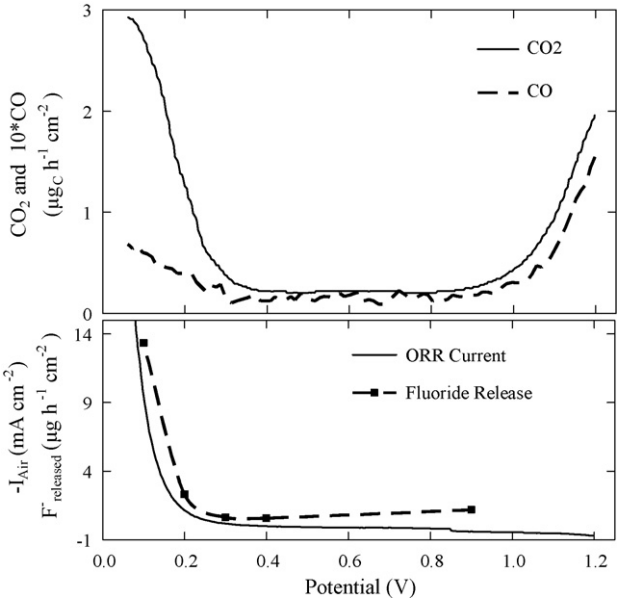

Fig. 3. CO_2 and CO evolution on pure carbon electrodes during potentiodynamic measurement in air (upper half of diagram). For simplicity only cathodic cycles are shown since anodic cycles barely differ (refer to Fig. 2). The lower part of the diagram shows the corresponding oxygen reduction current of the air measurement and the fluoride release rate which was measured in separate potentiostatic experiments.

Fig. 3 displays corrosion rates of pure carbon electrodes in air and corresponding oxygen reduction currents and fluoride release rates. The fluoride release was measured in separate experiments where the electrode was held at constant potential and collected cathode condensate was analysed with a fluoride selective electrode (ISE). Since the oxygen reduction activity of carbon is very low, an appreciable reduction current only can be observed below 0.3 V, i.e. at high overpotentials. The measured current is comparable to literature data in phosphoric acid provided by Kinoshita [32]. Parallel to the rise in reduction current an increasing fluoride release was observed. Fluoride release is generally correlated to ionomer degradation by peroxide radical attack [33,34], and serves as an indicator for the formation of hydrogen peroxide. Increase in fluoride release thus is considered as proof of hydrogen peroxide formation on pure carbon electrodes in air in the potential range of peak I.

Taking into account that hydrogen peroxide or peroxide radicals, respectively, are known to attack carbon [35] it is concluded that peak I in Fig. 2 can be ascribed to chemical carbon support oxidation according to the following reactions (8) and (9).

$$C \ + \ H_2O_2 \rightarrow \ C\text{–}O_{ad} + H_2O \qquad (8)$$

$$C\text{–}O_{ad} + H_2O_2 \rightarrow \ CO_2 + H_2O \qquad (9)$$

Corrosive chemical or electrochemical conditions lead to a higher surface coverage of oxide groups and an increase of surface defects on carbon [3,13,36]. It is known that acidic oxygen functional groups further diminish the poor peroxide decomposition capability of carbon and that quinone groups are involved

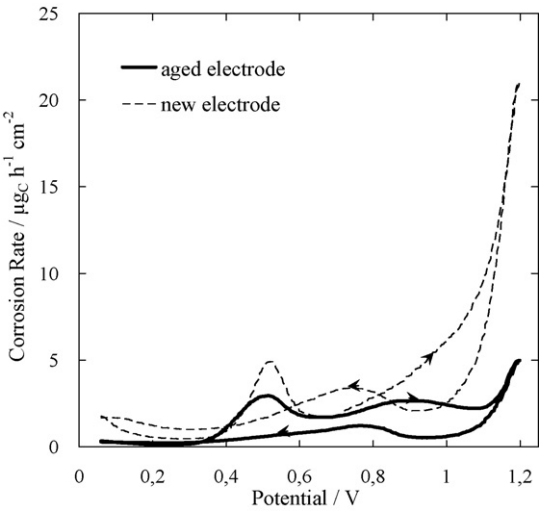

Fig. 4. Potentiodynamic corrosion measurements of an aged Pt/C-electrode compared to a new electrode.

in the formation of hydrogen peroxide [37]. Furthermore the increased platinum particle distance of aged Pt/C-catalysts reduces the probability of peroxide decomposition on adjacent catalyst particles and results in a higher apparent peroxide production in the potential region of peak I. Though these facts imply that enhanced peroxide production might result in increased carbon oxidation during peak I on aged electrodes, Fig. 4 shows that corrosion on the contrary is lessened on aged electrodes. This fact can be explained by decreased contact area of Pt-particle and carbon support and by diminished absolute carbon surface area due to carbon loss.

Peak II in the anodic cycle can only be found when Pt/C is used as catalyst and coincides with the potential for electrochemical oxidation of CO-adsorbates on platinum. Stripping experiments of CO conducted by Willsau and Heitbaum [18] and Roen et al. [19] and similar experiments conducted in our laboratory confirm that peak II is due to oxidation of Pt–CO_{ad} or CO_{ad}-like species in the proximity of platinum. Obviously these carbon oxides are formed at lower potentials than 0.55 V. This might be explained by chemical formation of oxygen functional groups on carbon by reaction (8) in the potential range of peak I. Another possibility is the observed formation of gaseous carbon monoxide which irreversible adsorbs on platinum at potentials below 0.55 V.

Peak V can be detected at Pt/C-electrodes. It is not very marked on new electrodes but can be very well detected on aged Pt/C-electrodes. Fig. 4 shows results with an electrode after heavy degradation during normal fuel cell operation. All features that were identified with new electrodes – namely peaks I–IV – still are clearly perceptible, though corrosion rates are much lower than with new electrodes. Peak V appears very pronounced on this electrode. Peaks I, III and IV are much less definite compared to a new electrode. This can be explained with platinum agglomeration lowering the contact area between catalyst and support. Furthermore a significant part of less stable carbon fractions is already oxidized and the defect density is lowered. Peak II is smaller because of decreased active catalyst area and reduced chemical carbon oxidation in the potential range of peak I. In [18] peak V was also identified and explained as an oxidation process of carbon surface oxides. It is reported in the literature that two different oxygen surface groups can form on carbon [38]. Elsewhere two surface oxides are reported, one being stable up to very high potentials and one being oxidized at normal cathode potentials [13]. Thus the oxidation process responsible for peak V can be ascribed to reaction (5) with surface oxygen being formed below 0.9 V according to (4) and being stable up to peak V. It has to be pointed out that peak IV – in contrast to the two-step process of peak V – takes place at such high overpotentials for carbon oxidation that steps (4) and (5) follow each other immediately.

In summary, five processes were identified on platinum-activated carbon electrodes that lead to evolution of carbon dioxide. As a consequence corrosion rates are increased in distinct potential ranges during transient operation.

4.2. Influence of potential characteristics

Fig. 5 shows dynamic corrosion experiments within different potential limits compared to measurements at constant potential. Corrosion rates in potentiodynamic mode are higher than those measured at constant potential. At constant potential only corrosion of that fraction of carbon is energetically feasible, which has a low enough activation energy. Furthermore oxide layers might build up which slow down corrosion rates [6]. A built-up of oxide layers stable up to 1.7 V was detected in Ref. [14] though the authors did not find an interaction with the oxidation process. Combination of these processes leads to a significant decrease of corrosion rate as long as the electrode potential is maintained unchanged (Fig. 6). Oxidation rates seem to have an asymptotic trend but do not fully level out.

With dynamic measurements high-corrosion rates exist even at steady-state conditions (usually after four to six repeated

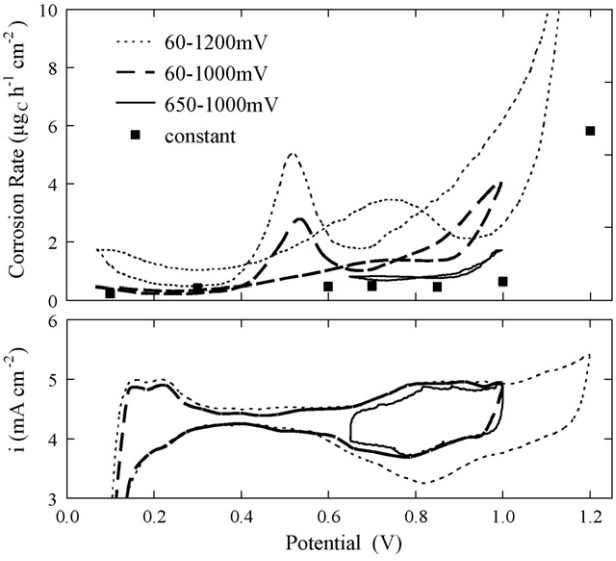

Fig. 5. Corrosion rates during dynamic and constant-potential measurements.

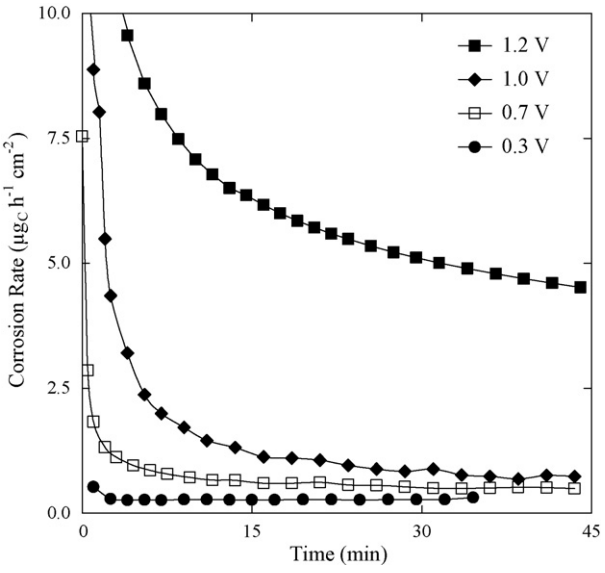

Fig. 6. Decay of corrosion rate at constant potential.

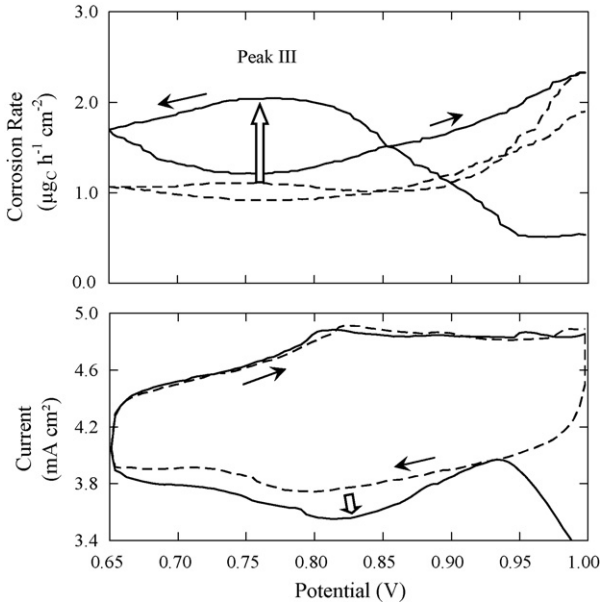

Fig. 7. Effect of 30 min exposure to high potential of 1.0 V and subsequent potential cycling (thick line). Small arrows indicate direction of potential sweep, thick arrows indicate increased OH-desorption and corrosion. Dashed lines are the respective second potential cycles which represent steady-state.

cycles) because time at high potentials is not long enough to build up irreversible oxide layers.

From Fig. 5 one can also deduce the dependence of corrosion rate on the upper and lower potential limit. The degree of carbon support oxidation increases with increasing anodic and with decreasing cathodic potential limit, respectively. This observation can be explained by strong electrooxidation at high overvoltage and by the creation of new defects by chemical oxidation in the low-potential region. Progressing from these newly generated defects, corrosion is lastingly enhanced even at less degrading potentials.

Another state of operation especially relevant for automotive application is long exposure to high potentials. In a car this situation occurs during stop-phases where the cathode is at or near open circuit potential (OCP), as simulated in Fig. 7.

After extended time at 1.0 V both the Pt–OH_{ad}-desorption area and the corrosion peak III are increased in the first potential sweep while reaching steady-state values in the subsequent cycles again. During exposure to the high potential an oxide layer with increasing thickness is built up on platinum. In the following cathodic sweep a higher amount of OH_{ad} is desorbed and promotes the corrosion process of peak III. This behaviour can also be seen as an additional proof for the origination of peak III as discussed in Section 4.1.

4.3. Influence of temperature and relative humidity

Figs. 8 and 9 show the dependence of carbon corrosion on humidity and temperature, respectively. Presented are the corrosion rates at the respective peak-maxima. Peak V is discarded because it can hardly be detected on new electrodes. Corrosion rates do only show linear dependence on molar water concentration. This finding implies that reaction (5), which requires one molecule of H_2O per molecule of CO_2 formed, is rate determining. Due to the clear sensitivity of carbon oxidation on humidity, care has to be taken when evaluating temperature dependence. First, relative humidity has to be unity at every temperature to prevent effects from partial drying out of the ionomer in the catalyst layer. Secondly, the molar water concentration has to be kept constant. These requirements can only be satisfied by adapting the system pressure as was done here. The Arrhenius type temperature dependency shown in Fig. 9 allows the calculation of activation energies. Values of 60.8 ± 4.1 and $57.9 \pm 3.4\,\mathrm{kJ\,mol^{-1}}$ are obtained for peaks III and IV, respectively. Peak II shows appreciably lower activation energy of

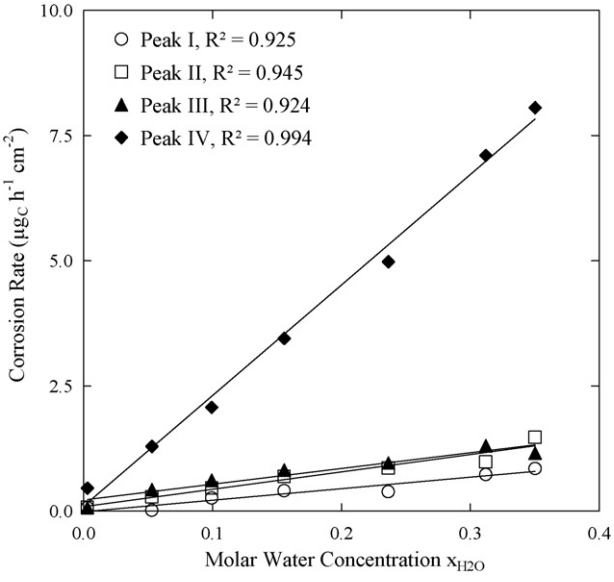

Fig. 8. Dependence of carbon corrosion rate on molar water concentration. Measurements were made by adapting relative humidity. Displayed are the respective peak maxima.

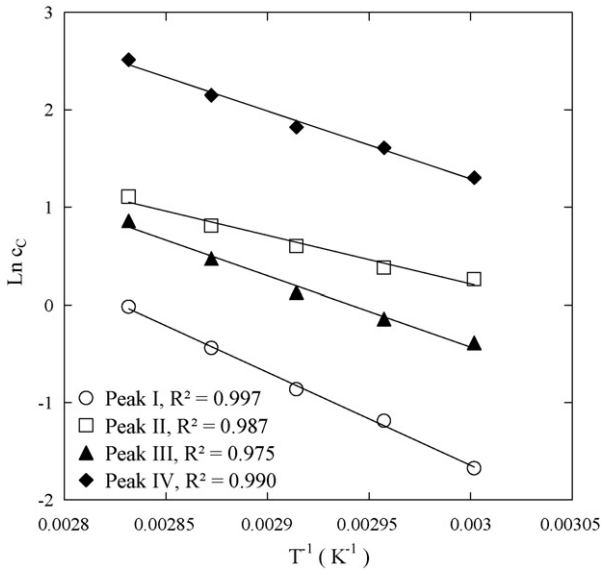

Fig. 9. Dependence of carbon corrosion rate on temperature at constant molar water concentration. Displayed are the respective peak maxima.

$41.4 \pm 3.8\,\mathrm{kJ\,mol^{-1}}$ since it is not ascribed to direct oxidation of the carbon support, but to oxidation of $Pt–CO_{ad}$. Differences in activation energies can be taken as another proof for above discussion concerning peak II. Chemical oxidation (peak I) exhibits an activation energy of $79.5 \pm 2.4\,\mathrm{kJ\,mol^{-1}}$.

4.4. Influence of graphitization

Since carbon corrosion has been identified as a crucial degradation mechanism especially in automotive applications, a lot of effort has been taken to develop carbon materials with a better corrosion stability. One approach is to use graphitized supports [11,22]. Graphitization generally is achieved by heat-treatment of high-surface area carbon blacks. This treatment leads to reduced surface heterogeneity and thus increased corrosion stability. Tests were conducted on electrodes with platinum supported on graphitized carbon. As graphitization only slows down kinetics of the carbon oxidation reaction but does not change the fundamental oxidation mechanisms, general features of dynamic measurements are the same as with Ketjenblack-based electrodes, only at lower oxidation rates.

5. Conclusions

The scope of the article is to present a dynamic measurement technique to evaluate carbon corrosion in PEM fuel cell cathodes. In contrast to earlier approaches, measurements were conducted in nitrogen and in synthetic air. This approach turned out to be essential to better understand corrosion mechanisms. It was shown that hydrogen peroxide formed on carbon support and platinum catalyst leads to increased corrosion at low potentials. The absolute value of the anodic potential limit strongly influences corrosion rates since new surface defects are formed at high potentials that subsequently can corrode at lower potentials. Exposure time to high potentials indirectly influences carbon oxidation by the formation of platinum oxide layers. Reduction of these oxides provides reactive oxygen species for the carbon oxidation reaction and leads to an increase in corrosion. Low cathodic potential limits increase oxidation rates by chemically forming new defects on the carbon surface. As a consequence of these processes, dynamic operation results in higher corrosion than constant-potential operation.

Carbon oxidation showed strong positive correlation with humidity and temperature, respectively.

The very complex dependence of carbon corrosion on degradation state, anodic potential limit, cathodic potential limit, exposure time to certain potentials – i.e. on the history of the electrode – and on temperature and humidity make it extremely difficult to predict corrosion in certain operation states or to predict time to failure under dynamic operating conditions. Further work will have to be done to develop a simple model to meet this requirement.

Acknowledgements

Colleagues at DaimlerChrysler AG, Department of MEA and Stack Technology are acknowledged for many discussions and support. Prof. Dr.-Ing. C. Merten is thanked for scientific supervision of this work.

References

[1] M. Pourbaix, Atlas of Electrochemical Equilibria in Aqueous Solutions, 2nd ed., Nat. Assoc. of Corrosion Engineers, Houston, Texas, 1974, Chapter IV, 17.1.
[2] E. Antolini, J. Mater. Sci. 38 (2003) 2995–3005.
[3] K.H. Kangasniemi, D.A. Condit, T.D. Jarvi, J. Electrochem. Soc. 151 (2004) E125–E132.
[4] A. Taniguchi, T. Akita, K. Yasuda, Y. Miyazaki, J. Power Sources 130 (2004) 42–49.
[5] K. Mitsuda, T. Murahashi, J. Electrochem. Soc. 137 (1990) 3079–3085.
[6] J.P. Meyers, R.M. Darling, J. Electrochem. Soc. 153 (2006) A1432–A1442.
[7] D. Yang, M.M. Steinbugler, R.D. Sawyer, L.L. VanDine, C.A. Reiser, US Patent 2003/0129462 A1.
[8] K. Mitsuda, T. Murahashi, J. Appl. Electrochem. 21 (1991) 524–530.
[9] C.A. Reiser, L. Bregoli, T.W. Patterson, J.S. Yi, J.D. Yang, M.L. Perry, T.D. Jarvi, Electrochem. Solid State Lett. 8 (2005) A273–A276.
[10] M.L. Perry, T.W. Patterson, C. Reiser, Electrochemical Society Transactions vol. 3(1), PEM Fuel Cell 6 (2006) 783.
[11] P.T. Yu, W. Gu, R. Makharia, F.T. Wagner, H.A. Gasteiger, Electrochemical Society Transactions vol. 3(1), PEM Fuel Cell 6 (2006), 797.
[12] E. Passalaqua, P.L. Antonucci, M. Vivaldi, A. Patti, V. Antonucci, N. Giordano, K. Kinoshita, Electrochim. Acta 37 (1992) 2725–2730.
[13] K. Kinoshita, J.A. Bett, Carbon 11 (1973) 237–247.
[14] G.A. Gruver, J. Electrochem. Soc. (1978) 1719–1720.
[15] M. Kiho, K. Matsunaga, S. Morikawa, O. Kato, Electrochemistry 69 (2001) 580–586.
[16] Z. Wei, H. Guo, Z. Tang, J. Power Sources 62 (1996) 233–236.
[17] D.A. Stevens, J.R. Dahn, Carbon 43 (2005) 179–188.
[18] J. Willsau, J. Heitbaum, J. Electroanal. Chem. 161 (1984) 93–101.
[19] L.M. Roen, C.H. Paik, T.D. Jarvi, Electrochem. Solid State Lett. 7 (2004) A19–A22.
[20] K. Kinoshita, Carbon, Electrochemical and Physicochemical Properties, Wiley & Sons, New York, 1988, p. 44.
[21] D.S. Cameron, S.J. Cooper, I.L. Dodgson, B. Harrison, J.W. Jenkins, Catal. Today 7 (1990) 113–137.
[22] E. Auer, A. Freund, J. Pietsch, T. Tacke, Appl. Catal. A 173 (1998) 259–271.

[23] F. Rodríguez-Reinoso, Carbon 36 (1998) 159–175.
[24] P. Stonehart, Progr. Batt. Solar Cells 5 (1984) 260–263.
[25] A. Binder, Electrochim. Acta 9 (1964) 255–274.
[26] A. Panchenko, M.T.M. Koper, T.E. Shubina, S.J. Mitchell, E. Roduner, J. Electrochem. Soc. 151 (2004) A2016–A2027.
[27] U.A. Paulus, T.J. Schmidt, H.A. Gasteiger, R.J. Behm, J. Electroanal. Chem. 495 (2001) 134–145.
[28] M. Inaba, H. Yamada, J. Tokunaga, A. Tasaka, Electrochem. Solid State Lett. 7 (2004) A474–A476.
[29] N.M. Markovic, T.J. Schmidt, V. Stamenkovic, P.N. Ross, Fuel Cells 1 (2001) 105–116.
[30] C. Zinola, A.M. Castro Luna, W.E. Triaca, A.J. Arvia, J. Appl. Electrochem. 24 (1994) 119–125.
[31] E. Yeager, Electrochim. Acta 29 (1984) 1527–1537.
[32] K. Kinoshita, Carbon, Electrochemical and Physicochemical Properties, Wiley & Sons, New York, 1988, p. 368.
[33] R. Baldwin, M. Pham, A. Leonida, J. McElroy, T. Nalette, J. Power Sources 29 (1990) 399–412.
[34] M. Hicks, Fuel Cells Durability Conference, Washington, DC, December 8–9, 2005.
[35] K. Kinoshita, Carbon, Electrochemical and Physicochemical Properties, Wiley & Sons, New York, 1988, p. 362.
[36] Y. Ryu, S. Pyun, C. Kim, D. Shin, Carbon 36 (1998) 293–298.
[37] K. Kinoshita, Carbon, Electrochemical and Physicochemical Properties, Wiley & Sons, New York, 1988, p. 364.
[38] H. Wolf, R. Landsberg, J. Electroanal. Chem. 29 (1971) 255–260.